



HAL
open science

”Bacchus” Methodological approach for vineyard inventory and management. Chap.4: Textural and structural analysis

Gilles Rabatel, C. Debain, Carole Delenne, M. Deshayes

► To cite this version:

Gilles Rabatel, C. Debain, Carole Delenne, M. Deshayes. ”Bacchus” Methodological approach for vineyard inventory and management. Chap.4: Textural and structural analysis. ”Bacchus” Methodological approach for vineyard inventory and management”, European Commission, DG Research, RTD Action: Energy, Environment and Sustainable Development, European Commission, DG Research, p. 67 - p. 87, 2006, 84-611-0107-3. hal-00448964

HAL Id: hal-00448964

<https://hal.science/hal-00448964>

Submitted on 20 Jan 2010

HAL is a multi-disciplinary open access archive for the deposit and dissemination of scientific research documents, whether they are published or not. The documents may come from teaching and research institutions in France or abroad, or from public or private research centers.

L’archive ouverte pluridisciplinaire **HAL**, est destinée au dépôt et à la diffusion de documents scientifiques de niveau recherche, publiés ou non, émanant des établissements d’enseignement et de recherche français ou étrangers, des laboratoires publics ou privés.

in : *"Bacchus" Methodological Approach for vineyard inventory and management*. Salomon Montesinos Aranda & Antonio Quintanilla (Eds). 2006. European Commission. DG Research. RTD Action: Energy, Environment and Sustainable Development., pp. 67-87

4. Textural and structural analysis

G. Rabatel, C. Debain, C. Delenne, M. Deshayes,
Cemagref, UMR ITAP & UMR TETIS, Montpellier (France)

4.1. Introduction

This chapter presents the methodologies that have been developed during the Bacchus project concerning the automatic detection and characterisation of vineyard plots in aerial images based on their structural properties, as well as the main results obtained in representative test areas of the project. They include a segmentation stage based on textural and shape criteria, followed by a more precise characterisation of the detected vineyard parcels.

Three main steps are defined: i) various textural criteria, based on co-occurrence matrices, are computed in order to determine the probability of any pixel to be a vineyard pixel. ii) this probability information is combined with geometrical and regularity constraints on the parcel shape to achieve the image segmentation, by means of active contours. iii) finally, the last step of characterisation, based on a Fourier analysis, also helps in revising the parcel enumeration. In the following, we present successively these various steps.

4.2. Textural analysis

4.2.1. Textural parameters

Texture analysis is a branch of image processing that began to be studied thirty years ago. Although the concept of texture was difficult to define (and is always), studies showed that spatial statistics computed on the grey levels of images were able to give good descriptors of the perceptual feeling of texture (for a review, see Haralick et al, 1973). Such textural descriptors are still developed today for classification tasks or segmentation problems (Ojala et al, 1996). In the present case, we have adapted the textural approach to satellite and aerial images, which present red (R), green (G) and near-infrared (NIR) channels.

The textural analysis is based on co-occurrences matrices. A co-occurrence matrix is the histogram, in a given neighbourhood for each pixel (e.g. 16x16), of the grey-level transitions when considering a given translation in a given direction.

For K possible grey-levels, it consists of a KxK bidimensional array, on which various parameters can be computed (Haralick et al, 1973).

In our case, we consider 8 elementary translations $(x,y) \rightarrow (x + \Delta x, y + \Delta y)$ where:

- (x,y) are the pixel coordinates
- $(\Delta x, \Delta y) \in \{ (1,0), (1,1), (0,1), (-1,1), (-1,0), (-1,-1), (0,-1), (1, -1) \}$
- $K = 32$ (number of grey level classes).

The 8 corresponding co-occurrence matrices are then summed up to obtain a unique matrix $M(i,j)$ ($0 \leq i < K$ and $0 \leq j < K$).

Five Haralick parameters are then computed as defined in Table 4.1.

Table 4.1. Definition of Haralick parameters ($M(i,j)$): KxK co-occurrence matrix)

| | |
|---|--|
| Energy: $E = \sum_i \sum_j (M(i, j))^2$ | Directivity: $D = \sum_i M(i, i)$ |
| Correlation: $Cor = \frac{1}{\sigma_i \sigma_j} \sum_i \sum_j (i - \mu_i)(j - \mu_j) M(i, j)$ <i>where μ_i, σ_i (resp. μ_j, σ_j) are the mean and standard deviation of $M(i,j)$ on the line i (resp. on the row j).</i> | |
| Entropy: $H = \sum_i \sum_j M(i, j) \log(M(i, j))$ | Contrast: $C = \sum_{k=0}^{K-1} \left(k^2 \sum_{ i-j =k} M(i, j) \right)$ |

Let us consider now a multispectral image, coded on n channels $C_1, C_2, \dots, C_u, \dots, C_n$. The previous co-occurrence matrix definition can be extended for any pair of channels (C_u, C_v) by counting the transitions from grey levels in channel C_u to grey levels in channel C_v , which is leading to an histogram array $M_{u,v}(i,j)$ ¹.

The pairs of channels that we have considered are (NIR,NIR), (R,R), (G,G), (NIR,R), (NIR,G), (R,G). We also compute the five Haralick parameters on the NDVI index given by :

¹ The case $u=v$ corresponds to the standard co-occurrence matrix for the channel C_u .

$$NDVI = \frac{NIR - R}{NIR + R} \quad (1)$$

This finally leads to 35 different textural features (7x5). Some examples of such computations are given in Figure 4.1.a (see the original image in *Figure 4.1.b*, in Annex): each feature is represented as a new image, which is normalised and can be used to compute multivariate criteria.

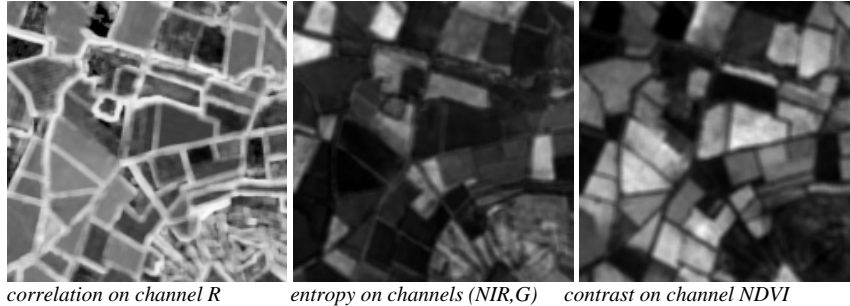


*Figure 4.1.a. Representation of some textural features
(original image in Figure 4.1.b in Annex)*

4.2.2. Vineyard probability index computation

A multivariate algorithm has been developed to combine the textural features described above into a vineyard probability index, that reflects the probability that a pixel belongs to a vineyard area or not. It is based on a Discriminant Factor Analysis which chooses the best textural features and/or their linear combination according to vineyard and non-vineyard classes.

The resulting value for a pixel is in the interval [0,1], the lower values corresponding to the highest vineyard probabilities (*Figure 4. 2*).

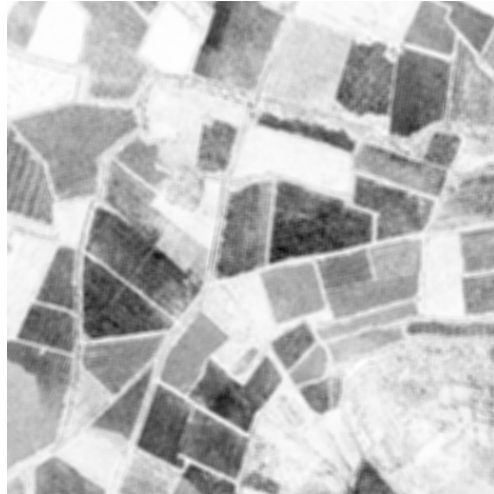


Figure 4.2. Vineyard probability index computation on “Bassin du Roujan”, France: darker areas correspond to a higher vineyard probability (original image in Figure 4.1.b, in Annex)

4.3. Parcel segmentation and characterisation

4.3.1. Methodological choices

In the previous part, various textural criteria have been considered, their purpose being to highlight the image areas which exhibit a vineyard structure. However, such a local approach is often insufficient to make a satisfactory segmentation, due to remaining ambiguities in some image areas. More global considerations, such as the homogeneity and shape regularity of the parcels, are then required.

For this reason, the parcel segmentation procedure is based on the grey-level probability image computed above (noted I in the following), in which each pixel value represents a probability of belonging to a vineyard rather than an actual textural classification result. Various approaches for region identification can be considered at this stage. Anisotropic diffusion (Perona & Malik, 1990) attempts to smooth local grey-level heterogeneities while preserving edges in the image. Region-growing algorithms, such as the Union-Find (Fiorio & Gustedt, 1996), allow labelling of homogeneous sub-areas (oversegmentation), which then can be merged according to shape criteria.

In the present study, however, we have chosen an edge-based approach, the *geodesic active contours*, because it facilitates the introduction of regularity and shape constraints on the boundaries of the detected objects. Geodesic contours

have been introduced by Caselles et al. (1997) as a new formulation of the classical “snakes” (Kass et al. 1988). They are based on the generic work of Osher and Sethian (1988) on front propagating curves. We have added “region forces”, as proposed by Paragios and Deriche (1999) in order to take better advantage of the probability image information. Finally, a *contour shape analysis* has also been implemented during the process, introducing more global shape criteria.

4.3.2. Geodesic Active Contours implementation

Geodesic contours rely on the idea that active contours can be seen as minimum length curves (or geodesics) in the image I , according to the particular metrics $g_1(x,y)$. If $g_1(x,y)$ is nearly null in the high gradient areas of I , these contours will naturally follow the salient edges in the image, in order to minimise their length. Minimisation problems related to active contours are usually solved iteratively, using a time differential equation to guide the curve evolution toward the solution (starting from an initial position). But in the case of geodesic curves, a level-set implementation becomes possible: curves are considered as the intersection of a 2D functional, the Ψ function, with the horizontal plane $Z=0$. A differential equation is then applied on the Ψ function, rather than on the contours themselves, to converge to the solution. Therefore, topological changes can occur during the process (Figure 4.3).

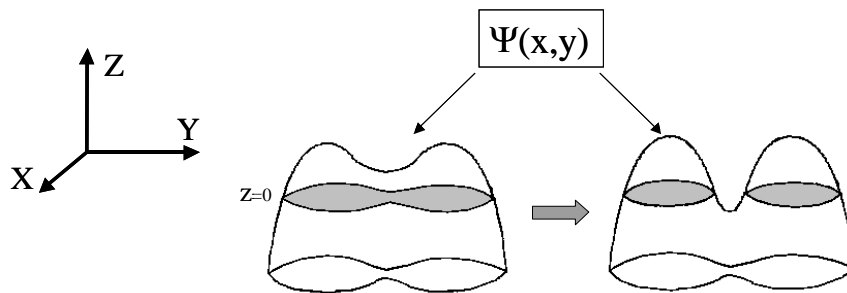


Figure 4.3. Topological change of active contour by level-set implementation

The initialisation of $\Psi(x,y)$ is not critical, because of these possible topological changes. In our case, it is determined in such a way that the corresponding initial contours ($\Psi(x,y) = 0$) draw a grid of “seeds”, in order to be sure to reach every vineyard parcel edge during the contour propagation.

Our “metric function” (or distance function) g_I is defined by:

$$g_I(x, y) = \exp\left(-\frac{1}{10} \cdot \frac{|\nabla I(x, y)|^2}{\langle |\nabla I|^2 \rangle}\right) \quad (2)$$

where $|\nabla I(x, y)|^2$ is the square of the gradient of the image I at the considered pixel location and $\langle |\nabla I|^2 \rangle$ is its average for the whole image.

As in Paragios and Deriche (1999), a “region function” R_I has also been defined for every pixel (x, y) by:

$$R_I(x, y) = I(x, y) - s \quad (3)$$

where s is a tuneable threshold value. The role of R_I is to introduce the region forces which cause the active contours to expand themselves in the image areas containing pixels with values below the threshold s (high probability to be a vineyard area) and to retract themselves otherwise.

Finally, according to Caselles et al. (1997) and Paragios and Deriche (1999), we obtain the following evolution equation:

$$\frac{\partial \Psi}{\partial t}(x, y) = g_I(x, y) \cdot \kappa |\nabla \Psi| + \nabla g_I \cdot \nabla \Psi + \beta \cdot R_I(x, y) \quad (4)$$

where t is the time, κ is the curvature of the Ψ function, ∇g_I and $\nabla \Psi$ are respectively the gradient of g_I and Ψ , and β is a tuneable coefficient for the region force term.

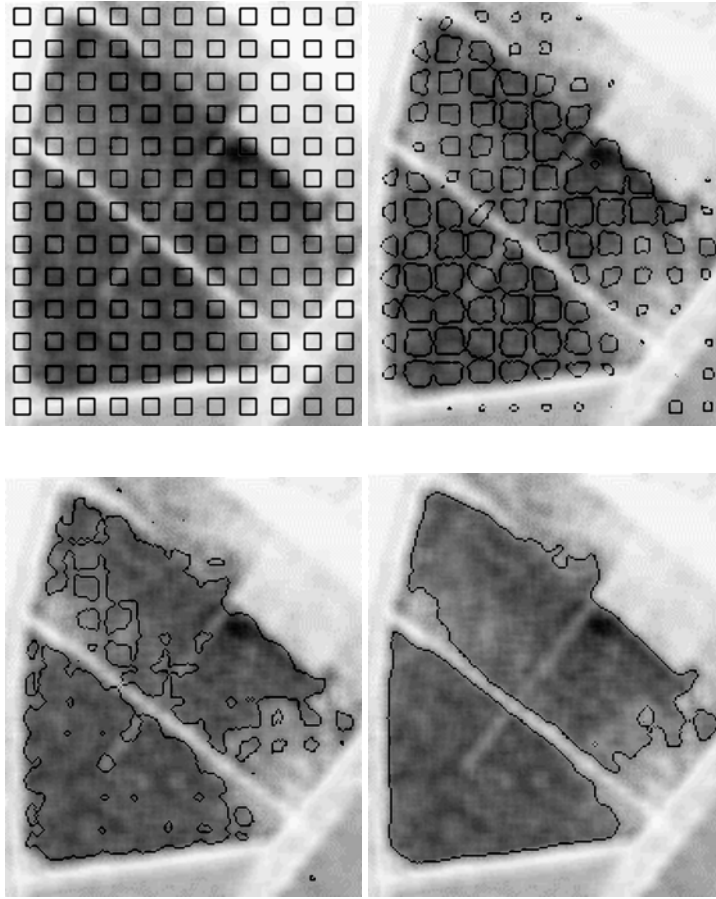


Figure 4.4. Contour evolution at various iteration steps

A discrete form of equation (4) is applied iteratively². Figure 4.4 shows an example of the active contours evolution at various iteration steps. The iterative process is automatically stopped according to a criterion based on the evolution speed of the total area of the negative parts of Ψ (i.e. of the total area of detected vineyard parcels, as according to the level-set implementation, the vineyard boundaries are given by $\Psi(x,y)=0$).

² At each iteration k : $\Psi_k(x, y) = \Psi_{k-1}(x, y) + \frac{\partial \Psi}{\partial t}(x, y) \cdot \Delta t$, where Δt controls the evolution speed

4.3.3. Region threshold management and contour shape analysis

The introduction of region forces in geodesic active contours allows us to select only parcel edges, rather than any grey-level transitions in the image. However, it requires definition of a threshold value s in equation (3) that should be well-adapted for the whole image, which brings us back to a very classical (and impossible to solve) binary segmentation problem.

To overcome this problem, the following scheme has been implemented:

- i). the whole process of geodesic active contour propagation is repeated with several increasing and arbitrary values of the threshold s .
- ii). at the end of each step, the boundaries of each detected parcel are analysed. The pieces of boundary that seem to correspond to real vineyard edges are then “locked” , so that they are not lost when applying further higher threshold values.

The basic idea of this boundary analysis is that parcel edges are generally quite long and rectilinear. Therefore, each parcel contour is first approximated as a polygon. Each polygon edge is then checked, according to its length, to the $g_i(x,y)$ values along its length and to the grey-level difference in image I between each of its sides. Moreover, an iterative relaxation procedure³ is then applied on the selected polygon edges, in order to optimise their position and their length before locking (Figure 4.5). The locking itself consists of artificially re-enforcing the image source grey-level on the external side of the contour.

Finally, when the higher threshold value has been applied, a list of detected parcels is produced in vector format. Figure 4.6 shows the result obtained at this stage, for the original image presented in Figure 4.1.b. Remaining segmentation errors are also indicated.

³ This relaxation procedure combines attraction by the low values of $g_i(x,y)$ and constant extension forces, the polygone edge being considered as a “rigid” snake.

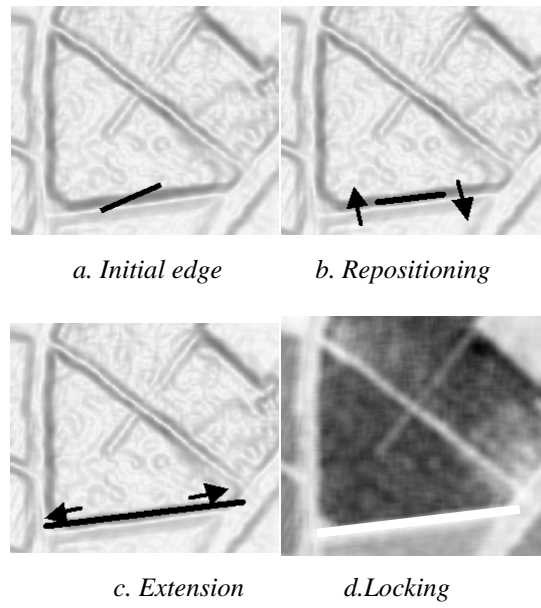


Figure 4.5. Edge relaxation and locking process
(a,b,c: image of $g_l(x,y)$ d: source image I)

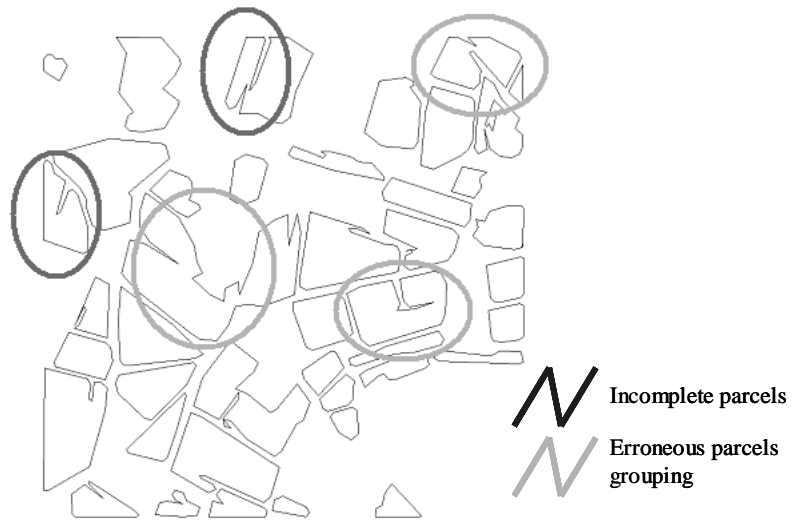


Figure 4.6. Vineyard parcel detection by geodesic active contours

4.3.4. Parcel revision and characterisation

Once the parcels have been detected, the last stage consists in determining some basic agronomic characteristics for all of them: distance between rows, orientation, etc. The inter-row and the orientation can easily be accessed by a Fourier analysis. However, some of the parcels identified by the previous step, due to detection errors, are made up of different parts with different characteristics. For this reason, the characterisation step includes a checking process, which allows revision of the parcel list.

The core of this checking process is a very selective bandpass filtering (Gabor filter), computed in the Fourier space. The main original point, compared to classical filtering approaches, is the following: because we start from a previously defined vineyard parcel candidate, we are able to set precisely the frequency and the orientation of the sinusoidal wave corresponding to the filter centre, and thus to be very selective. This filter centre is determined by looking for the amplitude peaks in the current Fourier spectrum, leading to a very efficient parcel selection, as illustrated in Figure 4.7.

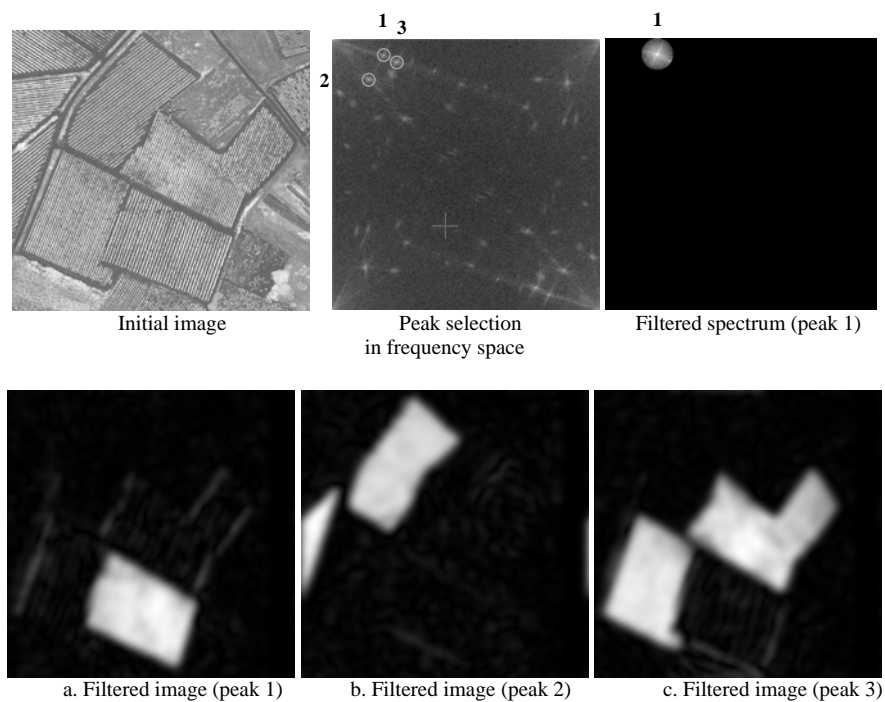


Figure 4.7. Vineyard parcel identification and characterisation based on a selective filtering process in the Fourier spectrum.

In order to identify every possible vineyard plot, the following recursive scheme is applied (Figure 4.8):

i) for each detected parcel from the initial list, its bounding box in the *original* aerial image (in grey-level) is considered and the corresponding Fourier spectrum is computed.

In this spectrum, various amplitude peaks are present and correspond to various periodical structures in the image. The peak with the maximal amplitude is selected as representing the characteristics of the considered parcel (inter-row distance and orientation).

ii) a sharp pass-band filter centred around this maximal peak is then applied so that the modulus of the inverse Fourier transform only highlights the image areas with the corresponding characteristics.

iii) every new object obtained is considered as a parcel, except if it intersects a bounding box edge. In this last case, a new bounding box is defined around this truncated object with an enlargement on the side where the object is incomplete, and the process is reiterated. By this way, the initial detected object can be completely recovered in a few steps.

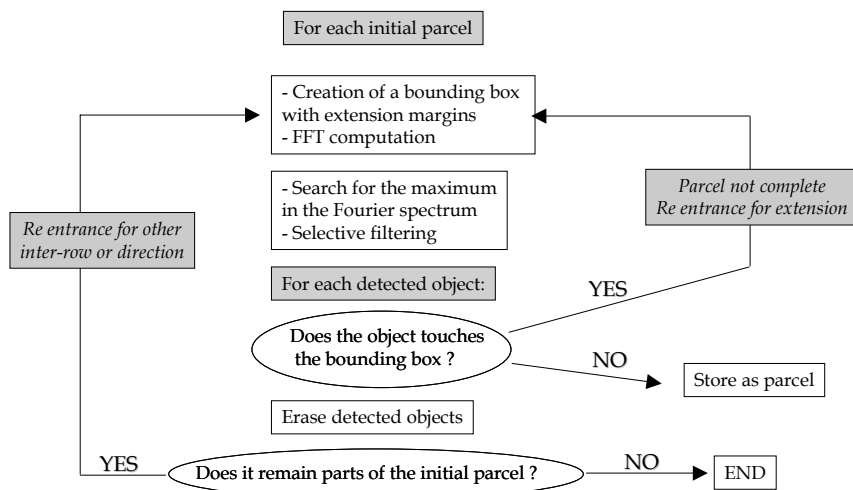


Figure 4.8. FFT based recursive scheme for parcel identification and characterisation.

iv) finally, the process is reiterated on the initial bounding box after erasing the new detected parcels, so that other significant Fourier spectrum peaks can be

selected and processed, to recover the parcels with different frequency or orientation.

A revised list of vineyard parcels is then produced, as shown in Figure 4.9.

The final outputs of the method are text files that give the number of vineyard parcels identified and for each parcel:

- its area,
- the position of its limits,
- the interrow distance,
- the row orientation.

In order to separate trellis (or wire trained) vines from goblet vines, additional information is provided. Goblet vines suppose the presence of one (in case of square planting) or two additional alignments (in case hexagonal planting). As a consequence, the software examines the frequency space and looks for additional peaks situated at 90° (for square planting) or at 60° and 120° (for hexagonal planting). It computes 3 ratios: ratio90, ratio60 and ratio120. Each ratio represents the ratio between the height of the maximum detected along this complementary orientation and the one of the initial and original peak. A later classification will decide whether ratio90 or both ratio60 and ratio120 are sufficiently high to qualify the detected vine as being trained in goblets.



Figure 4.9. Final result of parcel segmentation (vector format)

4.4. Evaluation of results

The results presented here have been obtained on two test sites of the Bacchus project, Limoux (Languedoc region, France) and Tarazona de la Mancha (Castilla La Mancha region, Spain). The Limoux test site has been selected as it is representative of vineyard areas where vines are predominantly grown with trellis. Furthermore the test site has been covered with two types of VHR data, aerial (AMDC data acquired by INTA) and satellite (QuickBird data). A second test site has been selected as representative of vineyard areas where vines are predominantly grown in goblets. This test-site is situated in Spain, near Tarazona de la Mancha.

4.4.1. *Data used*

The software for the segmentation of vine compartments has been tested with data extracted from two types of remote-sensing images of very high spatial resolution, INTA AMDC orthoimage and QuickBird panchromatic data. General information on the data available on the two sites are presented in Table 4.2..

Table 4.2. Remote-sensing data used for the segmentation of vine compartments for the Limoux (France) and Tarazona (Spain) test sites

| | INTA Limoux | QUICKBIRD Limoux | QUICKBIRD Tarazona |
|--|--|--------------------------------|-----------------------|
| Type | Aerial orthophotography | Satellite image | Satellite image |
| Date of acquisition | 29/05/2004 | 25/06/2002 | 31/07/2003 |
| Spatial resolution | 50 cm | 62 cm | 63 cm |
| Spectral bands used | Red, Near infrared and Panchromatic | Panchromatic | Panchromatic |
| Size of the extract | 4800 x 5300 pixels (636 ha) | 4000 x 4416 pixels (636 ha) | 2500x2500 pixels |
| Surface area of vine (photo- interpretation) | ≈290 ha (258 compartments) | ≈280 ha (257 compartments) | - |

4.4.2. Evaluation criteria

Four different levels of accuracy in vine detection can be distinguished:

1. Good detection (example on Figure 4.10, left):
 - The detected compartment and the real compartment share more than 80% of common surface area.
2. Average detection:
 - The detected compartment and the real compartment share more than 60% of common surface area.
 - a detected compartment groups together several real compartments (under-segmentation).
 - several compartments are detected for a single real compartment, and detected compartments share more than 60% of common surface area with the real compartment (over-segmentation, cf Figure 4.10, centre and right).

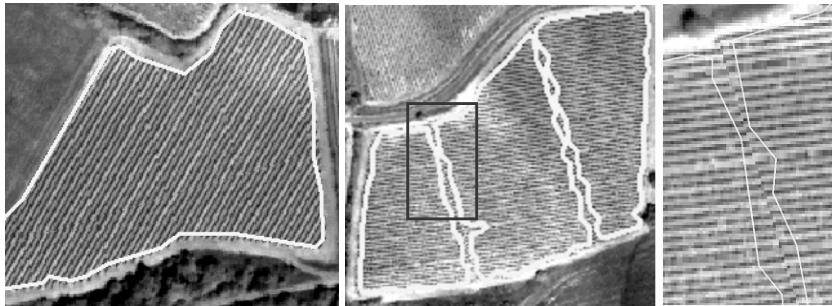


*Figure 4.10. Example of good detection (left) and over-detection because of a defect in the image (centre and detail, right)
Possible source: zone of assembling between two AMDC images*

3. Insufficient detection (example Figure 4.11):
 - The detected compartment(s) and the real compartment have less than 60% common surface area.
4. Non-detection

The first two levels constitute 'acceptable' detection of compartments.

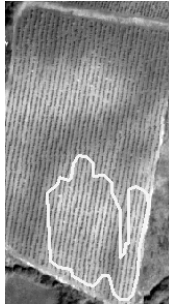


Figure 4.11. Example of insufficient detection

4.4.3. Results of vineyard plots identification and delineation on the Limoux test-site

Table 4.3 summarises the segmentation results on the Limoux test site for the two extracts of 636 ha presented in Table 4.2. Results are listed for each detection level as a percentage of the total number of compartments and a percentage of total surface area under viticulture. Illustrations of the precision of detection with the different data and bands are shown in annex, on Figure 4.12 to Figure.4.16.

Table 4.3. Results of the segmentation for the Limoux test site (percentage of compartments and surface area)

| | INTA Red (Figure.4.12, Annex) | | INTA NIR (Figure.4.13, Annex) | | INTA Red + NIR (Figure.4.14, Annex) | | INTA Pan (Figure.4.15, Annex) | | Quickbird Pan (Figure.4.16, Annex) | |
|-------------------------|-------------------------------------|----------------------|-------------------------------------|----------------------|--|----------------------|-------------------------------------|----------------------|--|----------------------|
| | % Plots | % Surface area | % Plots | % Surface area | % Plots | % Surface area | % Plots | % Surface area | % Plots | % Surface area |
| 1. Correct detection | 36 | 49 | 39 | 40 | - | - | 27 | 31 | 25 | 31 |
| 2. Average detection | 27 | 29 | 23 | 32 | - | - | 18 | 18 | 33 | 29 |
| 1+2: Acceptable | 63 | 78 | 62 | 72 | 79 | 91 | 45 | 49 | 58 | 60 |
| 3. Faulty detection | 15 | 9 | 8 | 9 | - | - | 23 | 31 | 10 | 17 |
| 4. Non detection | 22 | 13 | 30 | 19 | - | - | 32 | 20 | 32 | 23 |
| 3+4: Unacceptable | 37 | 22 | 38 | 28 | 21 | 9 | 55 | 51 | 42 | 40 |

4.4.4. Results of vineyard plots identification and delineation on the Tarazona test-site

The Tarazona test site is interesting because complementary to the Limoux test site, due to the dominance of goblet vineyards. The results of vine identification and delineation are shown on Figure 4.17 and details of this segmentation on Figure 4.18. They show that detection of goblet vineyards is operative. However the detection is limited by certain characteristics of the test-site (heterogeneity of soil and vine plants development, contrast or absence of contrast of field borders with neighbouring area). These points will be discussed below.

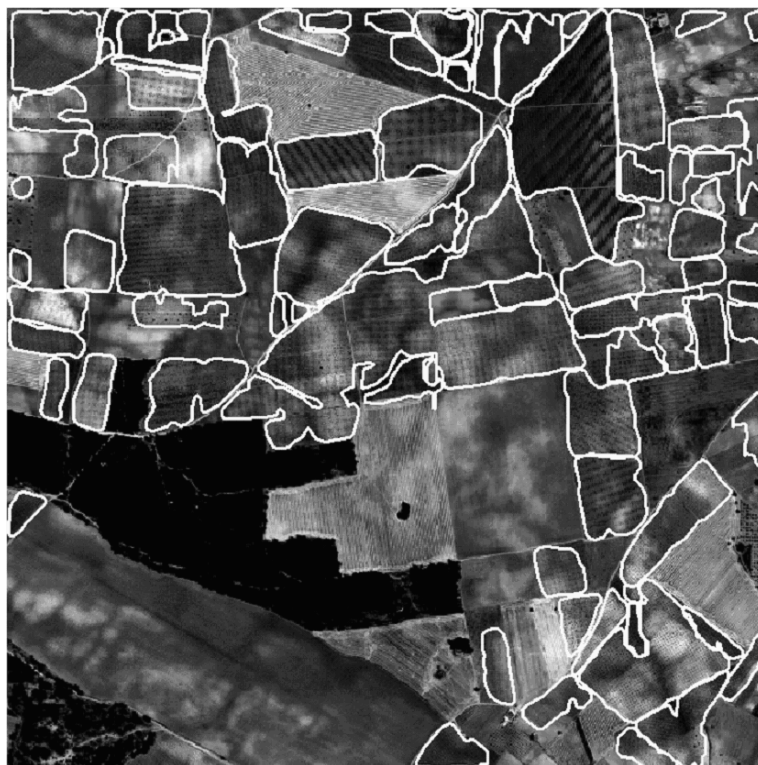


Figure 4.17. Result of the segmentation on the panchromatic channel of the Quickbird image, 2500x2500 pixels extract, Tarazona test-site (Spain)

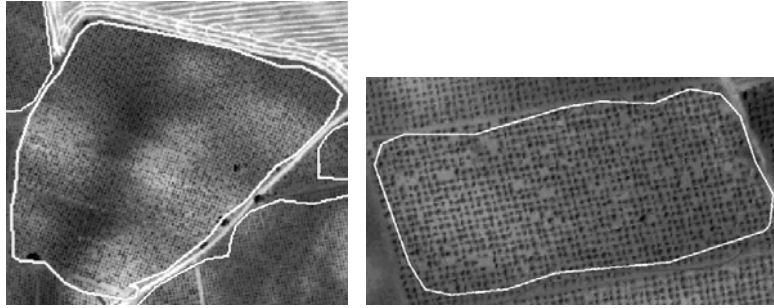


Figure 4.18. Details of segmentation on goblet vineyards, Quickbird image, Tarazona test-site (Spain)

4.4.5. Results of vineyard plots characterisation

Once a vineyard has been identified and delineated, it is de facto in the same time characterised, and with a good quality. Indeed if the parcel has been identified, it means that a significant peak is present in the frequency space, and through its polar coordinates (θ, r) this peak provides the information on interrow distance (related to r via the pixel size) and row orientation (θ). It should be kept in mind however that the precision in the determination of these parameters depends on the size and homogeneity of the plot: smaller and less homogeneous plots will lead to less precise parameters. Anyhow the user demand for precision in these parameters is not to the cm and the degree. A last remark is related to the identification of goblets. Once again, badly maintained goblet vines cause problems: when they are identified as vineyards, they are more liable to be not recognised as goblets and to remain identified as trellis.

4.4.6. Causes of errors in detection

The following causes of errors in detection have been identified: heterogeneity within the plot, young vines, detection of artefacts and bad detection of certain goblet vines. Details related to these faulty detections are presented hereafter.

a) Heterogeneity of the plot

The heterogeneity of the compartment is the major cause of bad detection. It can have several origins:

- Differences in vine vigour within the compartment (Figure 4.19, left), often caused by differences in supply of water and nutritional elements, themselves related to the terrain contours.

- Heterogeneity in the soil colour: soils with a clear colour provide a better contrast with vegetation in the visible bands whereas darker ones lead to less contrast (see an example on Figure 4.19, right). However areas with darker soils may appear more contrasted in the near infrared domain.

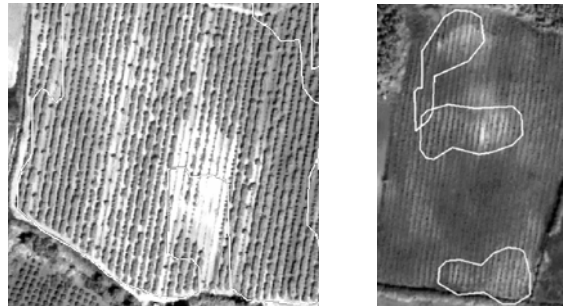


Figure 4.19. Problem of detection caused by heterogeneities of vine vigour. Left: heterogeneity of vine vigour, the area devoid of vegetation is excluded from the vineyard. Right: heterogeneity of soil colour: only the areas that are the most contrasting are detected.

b) Young vines

Some vines are not detectable because their level of soil coverage is low. These are most notably young vines (*'plantiers'* in French), one or two years old (Figure 4.20),

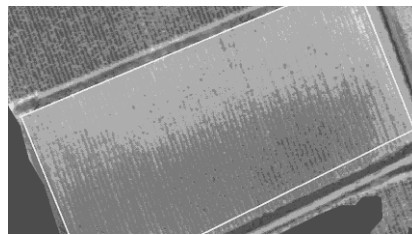


Figure 4.20. Example of a young vine: the rows are barely discernible

c) Detection of non-vine

It is very rare for a compartment to be detected where there is no vine. Whenever this happens, it is often due to ditches between two compartments or roads that present an oriented texture (Figure 4.21). The latter case of false detections may be later suppressed through post processing.



Figure 4.21. Example of non-vine (here a highway) detected as vine

d) Vines trained as goblets

On the Limoux test site, vines trained as goblets i.e. pruned as bushes (untrained vines) are not easily detectable for at least three reasons. Firstly these vines are generally old (50 years and above), and generally not very well maintained, with a high level of missing vine plants. Furthermore the vines are not trimmed, which leads to a lower contrast, and finally they are grown on small plots (Figure 4.22). In the Limoux area, where the profession is dynamic and most of these vineyards have been uprooted and replanted with higher quality varieties, these goblet vineyards represent only 2 to 3% of the total.

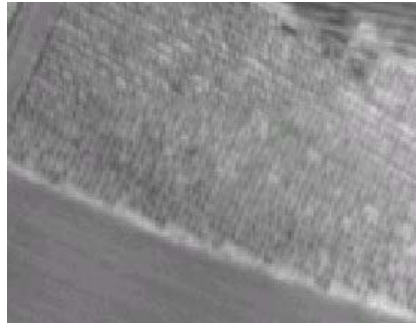


Figure 4.22. Example of vine trained as goblet (Limoux)

4.4.7. Analysis and interpretation of results

From the analysis of the above results, the following comments can be made:

- With good conditions of contrast, the detection of vineyards, either in trellis (as in Limoux) or in goblets (as in Tarazona), is operative

- Very few non-vine compartments were detected as vine (see a counter example on Figure 4.21).
- Results are always better for surface area than for the number of compartments. In fact, compartments that were incorrectly detected or non-detected are usually the very smallest ones.
- Panchromatic channels do not seem to be suitable for detecting viticulture compartments in the Limoux region.
- In spite of the slightly lower resolution of the Quickbird image, its results are distinctly better than those from the panchromatic channel of the INTA image. This can perhaps be explained by the fact that Quickbird's panchromatic channel covers a wider spread of wavelengths, in particular for the near infrared, when compared with the panchromatic channel of the INTA image, which only covers the wavelengths of the visible domain.
- On the Limoux test-site, the best results are provided by processing the red channel. However, the results of the processing on the near infrared channel are complementary: **79% of compartments (91% of viticulture surface area) are detected by the red channel and the near infrared channel** (Table 4.3). The use of the panchromatic channel does not lead to any additional improvements.
- The presence of a certain heterogeneity on the vineyards borders, with lower contrast (vine plants of lower vigour) or gaps in the row (missing plants) is not favorable to a reliable definition of the parcel limits. In order to obtain more representative limits, a specific post-processing step would be necessary.

Some incorrect detection can also be explained by an insufficient image resolution, specially for inter-row widths smaller than 2 m. Figure 4.23 shows an example of segmentation of an image of 20 cm resolution, obtained by Cemagref using an ULA. In this case, for a total of 20 compartments, only one was not detected, one was incorrectly detected, and there were two groupings of compartments.

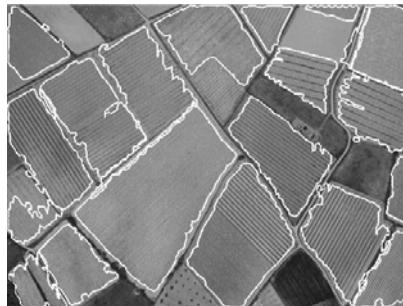


Figure 4.23. Example of segmentation of an ULA image of 20 cm resolution

4.5. Discussion and conclusion

In the Limoux region (and the corresponding appellation zone) and in the Tarazona region, there is an overall homogeneity of vines, with, in particular, the inter-row or inter-plant distances being generally greater than 2 m. These distances are specific to the vine in the region, other crops grown in rows (maize, sunflower..) having a much smaller separation (0.80 m) and there is no possibility of confusion. With these kinds of patterns, the algorithm developed in the Bacchus project is generally operative.

The causes of insufficient detection have different origins. The first cause is heterogeneity in vine appearance. This heterogeneity depends on terrain contours, soil colour, soil depth and the relative supply of water and nutrients, all these factors being tightly interlinked. Yet another factor for heterogeneity is related to crop practices (tillage and/or total or partial weeding). Secondary causes of bad detection are the small size of plots (not favourable for obtaining a 'good' Fourier transform), young vines (less than two or three years old) and bad level of vine maintenance (numerous missing vine plants, 'dirty' vines, as with the old goblets vineyards in France).

As a consequence, the methodology developed in the Bacchus project can produce good results, as on the Limoux test site, where 91% of the viticulture surface area has been detected. However these results directly depend on a good legibility of vineyards on the original remotely sensed images and cannot be generalised without taking a few precautions. And in any case they require a visual post-processing to correct detection defects before inclusion in the GIS data base.

4.6. References

- Caselles, V., R. Kimmel, G. Sapiro 1997. Geodesic active contours. *International Journal of Computer Vision* 22(1) 61-79.
- Fiorio, C. and J. Gustedt 1996. Two linear time Union-Find strategies for image processing. *Theoretical Computer Science* 154(1996) 165-181.
- Franklin, S.E., R.J. Hall, L.M. Moskal, A.J. Maudie, M.B. Lavigne 2000. Incorporating texture into classification of forest species composition from airborne multispectral images. *International Journal of Remote Sensing* 21(1) 61-79.
- Haralick, R. M., K. Shanmugam, I. Dinstein 1973. Textural Features for Image Classification. *IEEE transactions on systems, man, and cybernetics* 3(6) 610-621.
- Kass, M., A. Witkin, D. Terzopoulos 1988. Snakes : Active contour models. *International Journal of Computer Vision* 1(4) 321-331.

- Ojala, T., M. Pietikäinen, D. Harwood 1996. A comparative study of texture measures with classification based on feature distributions. *Pattern Recognition* 29 51-59.
- Osher, S. and J. A. Sethian 1988. Fronts propagating with curvature dependent speed: algorithms based on Hamilton-Jacobi formulations. *Journal of Computational Physics* 79 12-49.
- Paragios, N. and R. Deriche 1999. Geodesic Active Regions for Supervised Texture Segmentation. In: *Proceedings of the 7th IEEE Int. Conference on Computer Vision, ICCV '99; IEEE Comput. Soc.; Vol.1, 1999; pp. 926-32*
- Perona, P. and J. Malik 1990. Scale-space and edge detection using anisotropic diffusion. *IEEE Transactions on Pattern Analysis and Machine Intelligence* 12(7) 629-639.

ANNEXE

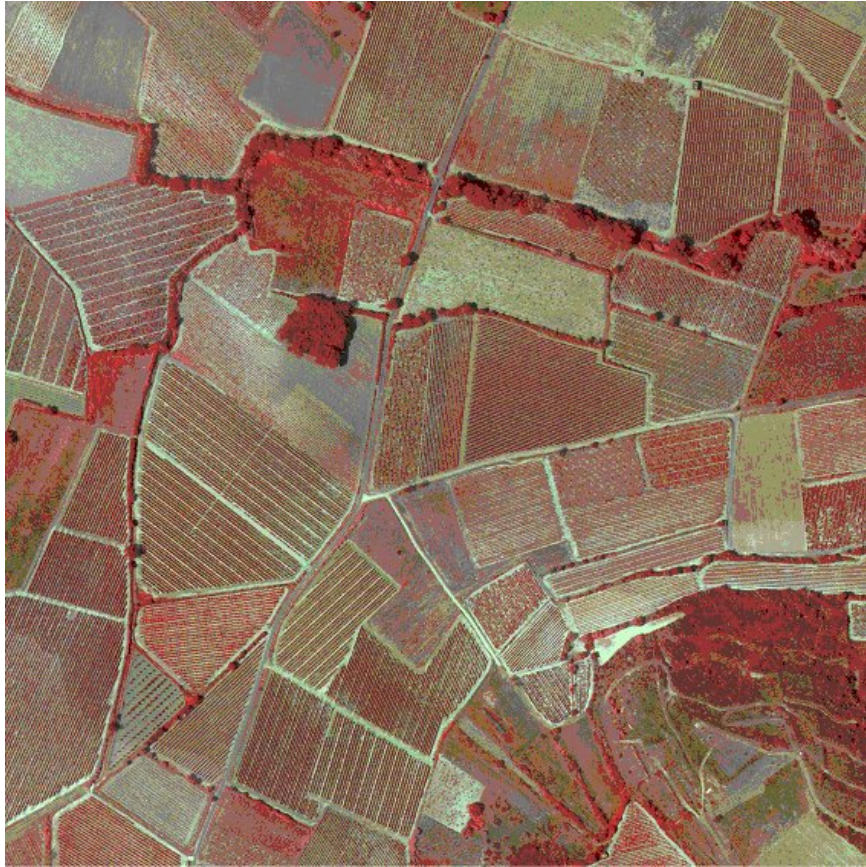


Figure 4.1.b. Original 50 cm resolution color infrared image used for algorithm development. Roujan area, Languedoc, France



Figure 4.12. Results of the segmentation on the red channel of the INTA image, Limoux test-site (France)

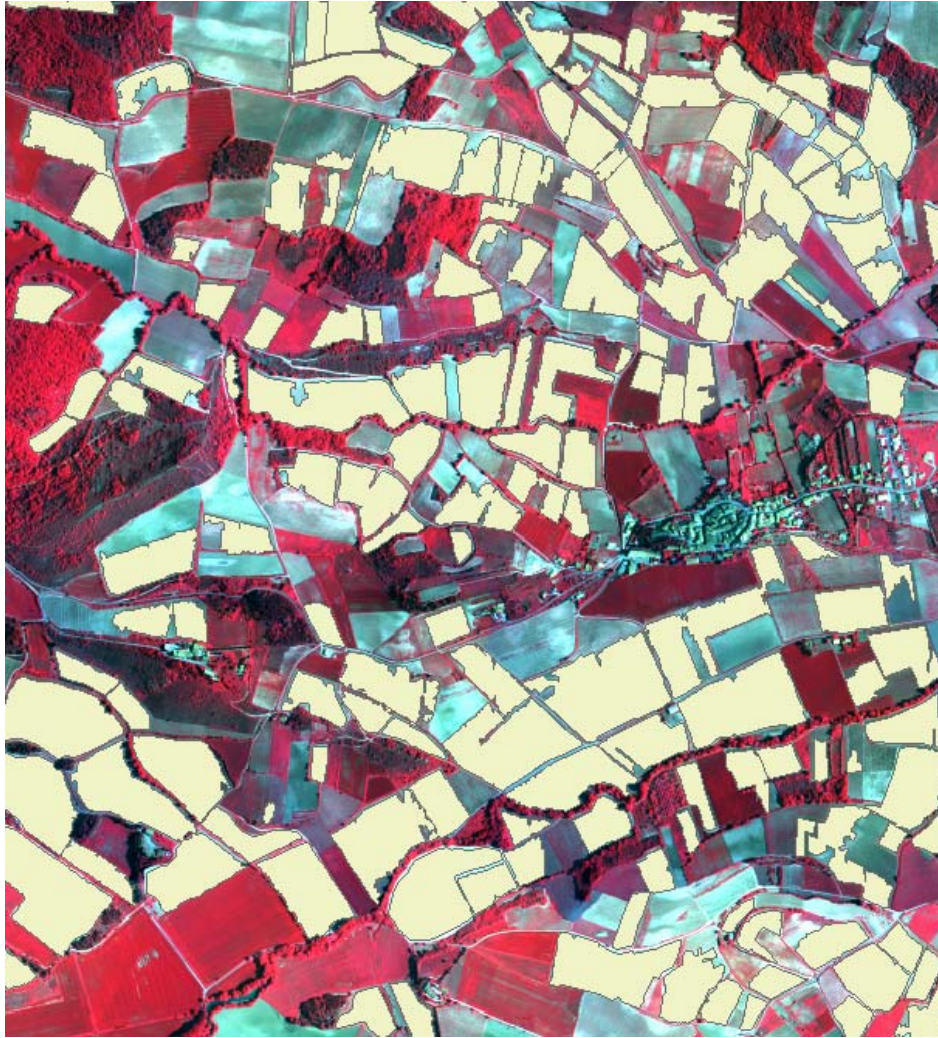
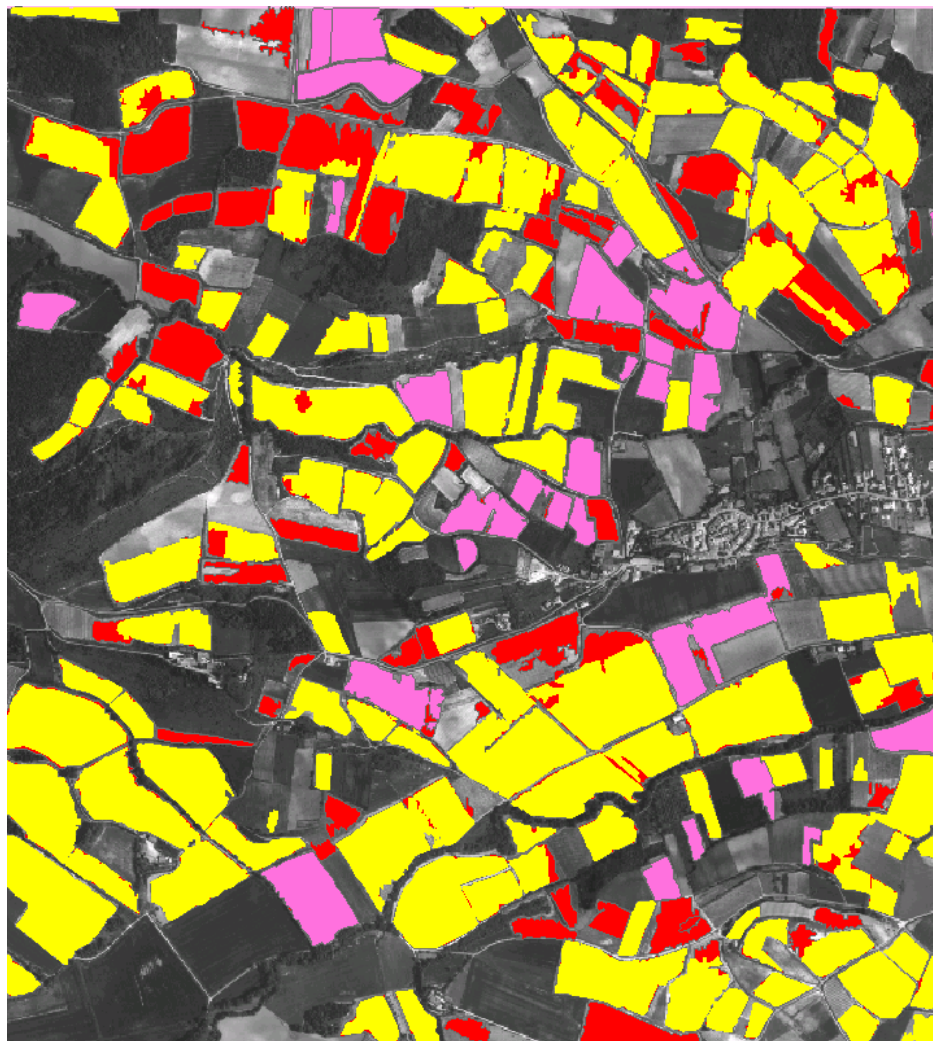


Figure.4.13. Results of the segmentation on the near infrared channel of the INTA image, Limoux test-site (France)






-  Plots detected with both bands
-  Plots detected with the red band only
-  Plots detected with the NIR band only

Figure.4.14. Complementarity of detection with the red and near infrared channels of INTA data, Limoux test-site (France)

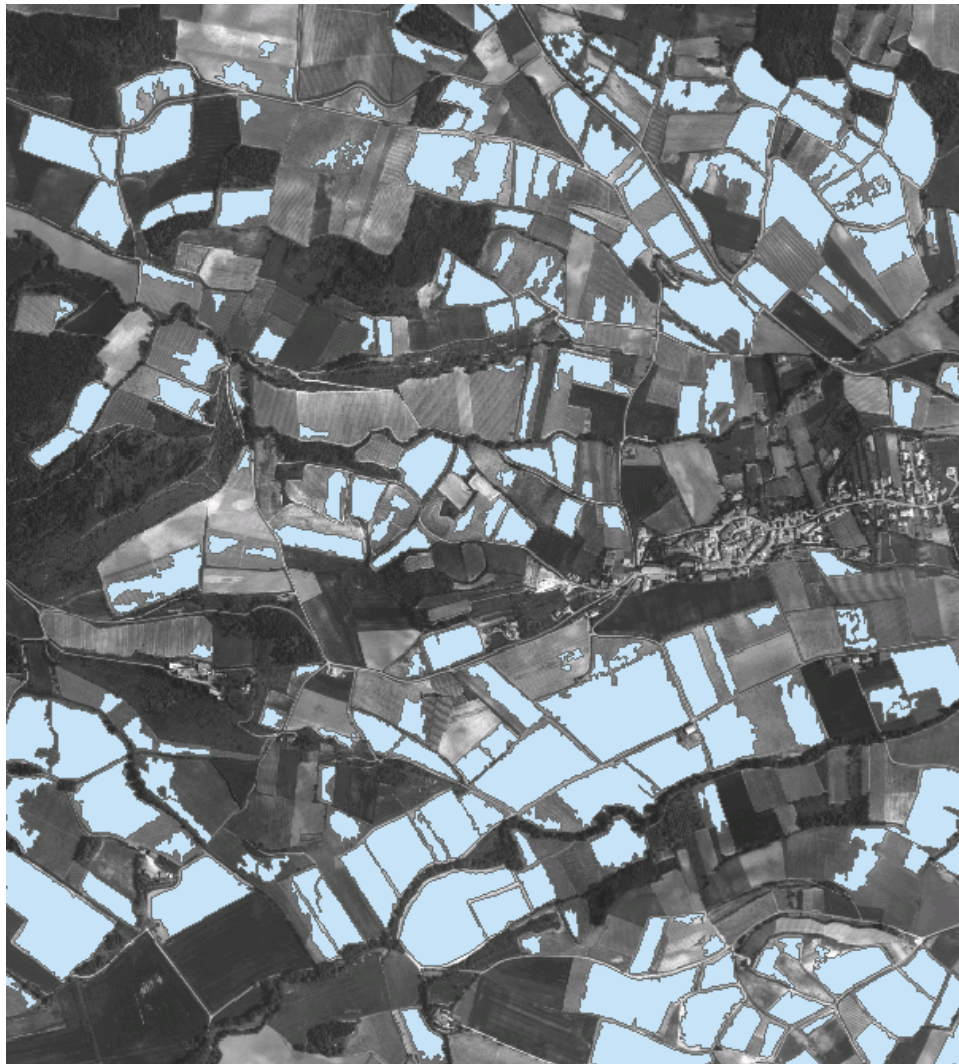


Figure.4.15. Result of the segmentation on the panchromatic channel of the INTA image, Limoux test-site (France)

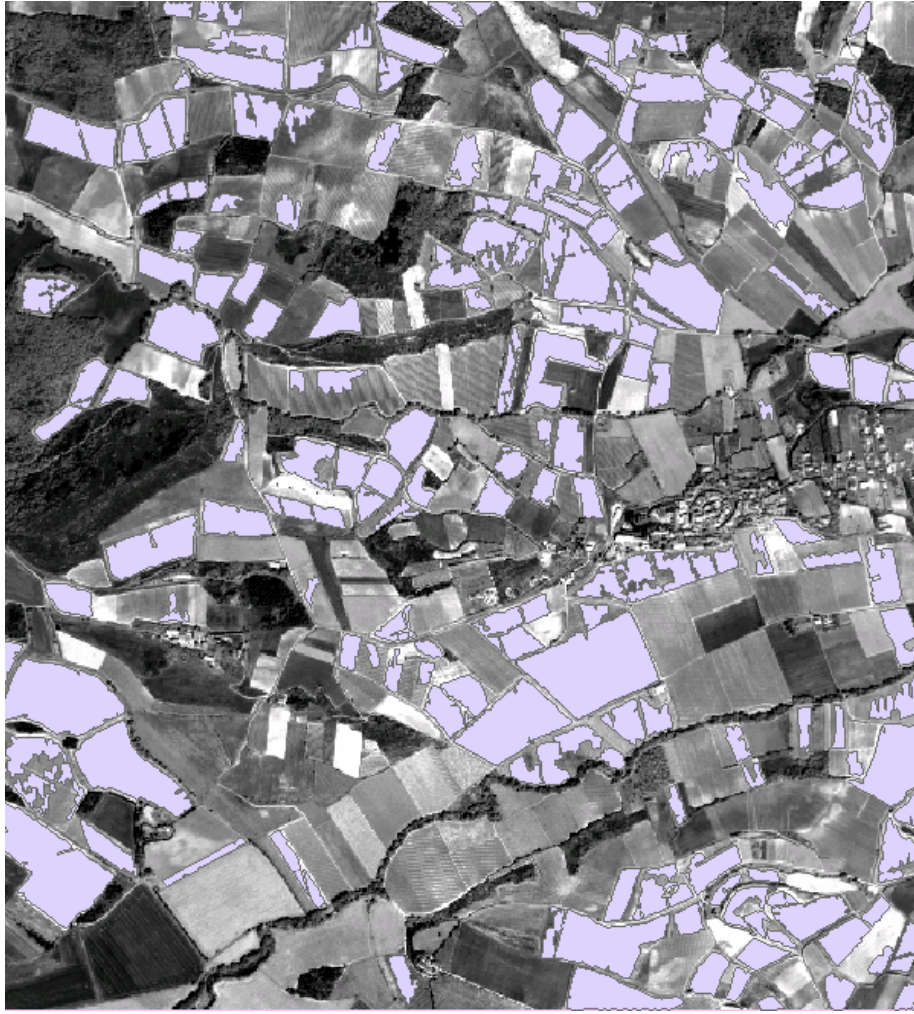


Figure.4.16. Result of the segmentation on the panchromatic channel of the Quickbird image, Limoux test-site (France)